

# Quantum Simulation of Quantum $\mathbb{Z}_2$ Gauge Theory demonstrated in a GPU Simulator

Xiaopeng Cui,<sup>1</sup> Ji-Chong Yang,<sup>1,2</sup> and Yu Shi<sup>1,\*</sup>

<sup>1</sup>*Department of Physics & State Key Laboratory of Surface Physics,*

*Fudan University, Shanghai 200433, China*

<sup>2</sup>*Department of Physics, Liaoning Normal University, Dalian 116029, China*

## Abstract

We outline a quantum simulation scheme of quantum  $\mathbb{Z}_2$  gauge theory using quantum adiabatic algorithm implemented in terms of quantum circuit, and then demonstrate it in the classical simulator QuEST using a CUDA enabled GPU server. In particular, we obtained useful results in (3+1)-dimensional and (2+1)-dimensional theories. It is identified that the quantum phase transition is topological in both dimensions, and is first-order in (3+1) dimensions but second-order in (2+1) dimensions. High-performance classical simulation of quantum simulation, which may be dubbed pseudoquantum simulation, is not only a platform of developing quantum software, but also represents a new practical mode of computation.

---

\* yushi@fudan.edu.cn

## I. INTRODUCTION

Quantum simulation and quantum computing, first conceived by Feynman, Deutsch and others, are under extensive studies worldwide, thanks to the rapid development of quantum science and technology. A controllable system, which may be even programmable, simulates another quantum system, which may be difficult to control, and the physical properties under different parameters can be conveniently studied. The algorithms of quantum simulations have become increasingly mature. The Trotter decomposition [1], the sparse Hamiltonian quantum walk [2], the dense Hamiltonian density matrix exponentiation [3–5], and the adiabatic evolution [6, 7] have paved the way to simulate lattice spin models. It becomes timely to develop quantum software [8]. An important possibility is to use quantum simulation to study lattice gauge theory [9–11], the major non-perturbative approach to gauge theory, which is the framework of standard model of particle physics, describing both electroweak and strong interactions, and is also important in condensed matter physics.

Lattice gauge theory has made great achievements using Monte Carlo (MC) simulations [12]. In presence of fermions, however, due to Grassmann numbers, the integrals may cause the partition function to change sign and oscillate violently, consequently the “importance sampling” in MC is no longer valid [13]. This is the notorious “sign problem” [14, 15]. Hopefully it can be avoided in quantum simulation, which is also an ideal avenue to study quantum phase transition (QPT) and quantum dynamics.

The simplest lattice gauge theory is the  $\mathbb{Z}_2$  gauge theory [16–19], which is the simplest case of  $Z_n$  theories, which can be obtained from discretizing  $U(1)$  theory.  $\mathbb{Z}_2$  gauge field can also be embedded or emerged in other models, such as  $\mathbb{Z}_2$  Higgs model,  $\mathbb{Z}_2$  spin liquid,  $\mathbb{Z}_2$  embedded Hubbard model, etc, which are closely related to topological phase transitions, high temperature superconductivity and fractional quantum numbers, etc. [12, 20].  $\mathbb{Z}_2$  toric code model can be regarded as a variant of quantum  $\mathbb{Z}_2$  gauge theory and plays an important role in topological quantum computing [21–23]. Quantum simulation of  $\mathbb{Z}_2$  gauge theory has been theoretically considered [24], while quantum simulation of  $\mathbb{Z}_2$  toric code model has been experimentally demonstrated [25, 26].

In classical  $\mathbb{Z}_2$  gauge theory, there is a phase transition without spontaneous breaking of any local symmetry [16, 17], called topological phase transition [19]. MC revealed that the phase transition is first-order in 4 dimensions, and is second-order in 3 dimensions

[27], suggesting that the quantum phase transition (QPT) in quantum  $\mathbb{Z}_2$  gauge theory is first-order in (3+1) dimensions, and is second-order (2+1) dimensions, since the classical statistical mechanics of a D-dimensional model corresponds to (d+1)-dimensional quantum model, where  $d=D-1$  refers to the spatial dimension, 1 refers to the time dimension. First-order QPT is an interesting issue [28]. Among others, it was observed experimentally in a dissipative quantum system[29], and in topological crystalline insulators[30]. It is also related to quantum adiabatic algorithm [31].

To perform quantum simulation of quantum  $\mathbb{Z}_2$  gauge theory, at least 25 qubits are needed in (3+1) dimensions, including one on each link on the  $d=3$   $2 \times 2 \times 2$  lattice and an ancillary qubit needed in the quantum algorithm, called ancilla. More qubits are needed for phase estimation and eigenvalue measurement algorithms. Tens of thousands of Trotter decomposition steps are required to implement the adiabatic algorithm. It is now still difficult for the experimental platforms to meet the requirements on the qubit number, error rate and coherence time. Therefore, it is interesting to simulate quantum simulation on classical high-performance computing platform. This may be called pseudoquantum simulation. It also facilitates the development of quantum software [8].

The latest graphics processing unit (GPU) parallel acceleration technology provides parallel computing architecture that greatly accelerates large-scale complex scientific computation. The GPU simulator QuEST, the Quantum Exact Simulation Toolkit, is a new software platform simulating the quantum circuit [32]. It is based on the software platform and application programming interface CUDA created by Nvidia, which allows software developers to develop parallel program with a CUDA-enabled GPU. Designed as a C library, QuEST allows quantum codes to be deployed in a variety of computing platforms. With high precision, it can simulate 29 qubits on a single Nvidia K40m GPU. It fits our need of pseudoquantum simulation of quantum  $\mathbb{Z}_2$  gauge theory.

In this paper, we present a scheme of quantum simulation of quantum  $\mathbb{Z}_2$  gauge theory using quantum adiabatic algorithm implemented in terms of quantum circuit, which is then simulated using QuEST in a Nvidia K40m GPU server. We study the model in (3 + 1) dimensions and (2 + 1) dimensions. In each dimension, we observe the QPT and determine its type, and confirm the topological nature in both dimensions. This work demonstrates the advantages of quantum simulation as well as its classical simulation in terms of a GPU-based simulator.

## II. QUANTUM SIMULATION

### A. Quantum $\mathbb{Z}_2$ Gauge Theory

The Hamiltonian of quantum  $\mathbb{Z}_2$  gauge theory is [19]

$$H = Z + gX, \quad (1)$$

with

$$X \equiv - \sum_l \sigma_l^x, \quad Z \equiv \sum_{\square} Z_{\square}, \quad (2)$$

where  $\square$  represents each elementary plaquette, as shown in Fig. 1,

$$Z_{\square} = - \prod_{l \in \square} \sigma_l^z, \quad (3)$$

the coupling constant  $g$  is the parameter to be tuned. For each qubit,  $\sigma^z|0\rangle = |0\rangle$ ,  $\sigma^z|1\rangle = -|1\rangle$ . The Hamiltonian of the classical  $\mathbb{Z}_2$  theory is  $Z$ , with the operators  $\sigma_l^z$  reduced as the classical variables. The quantum features of  $H$  is due to the noncommutativity between  $\sigma_l^x$  and  $\sigma_l^z$ , causing the competition between  $Z$  and  $X$ , in a way like that between energy and entropy in thermal phase transitions.  $g$  plays a role in QPT similar to the role of the temperature in thermal phase transition.

Depending on  $g$ , there are two different phases, deconfined and confined, separated by a QPT at the critical point  $g_c$ , where there is no spontaneous symmetry breaking, and one cannot find a local order parameter to characterize it. But one can use the behavior of the Wegner-Wilson loops to characterize it. There is  $\mathbb{Z}_2$  topological order in the deconfined phase, while the confined phase is trivial, hence it is a topological QPT [16, 19].

To simulate this theory, we first design the quantum adiabatic algorithm and the quantum circuit implementing the algorithm, in which  $g$  varies from 0 to a large enough value, passing  $g_c$ . Periodic boundary condition is assumed, that is, the lattice is on a torus. Each link is occupied by one qubit. The links and thus the qubits are numbered as in Fig.2. For  $D=(3+1)$  theory, the lattice is  $d=3 \ 2 \times 2 \times 2$ , where there are 24 links, 24 elementary plaquettes, and 25 qubits, one of which is the ancilla. For  $D=(2+1)$  theory, the lattice is  $d=2 \ 3 \times 3$ , where there are 18 links, 9 elementary plaquettes, and 19 qubits, one of which is the ancilla. Although the lattice sizes are small, all the key features do appear.

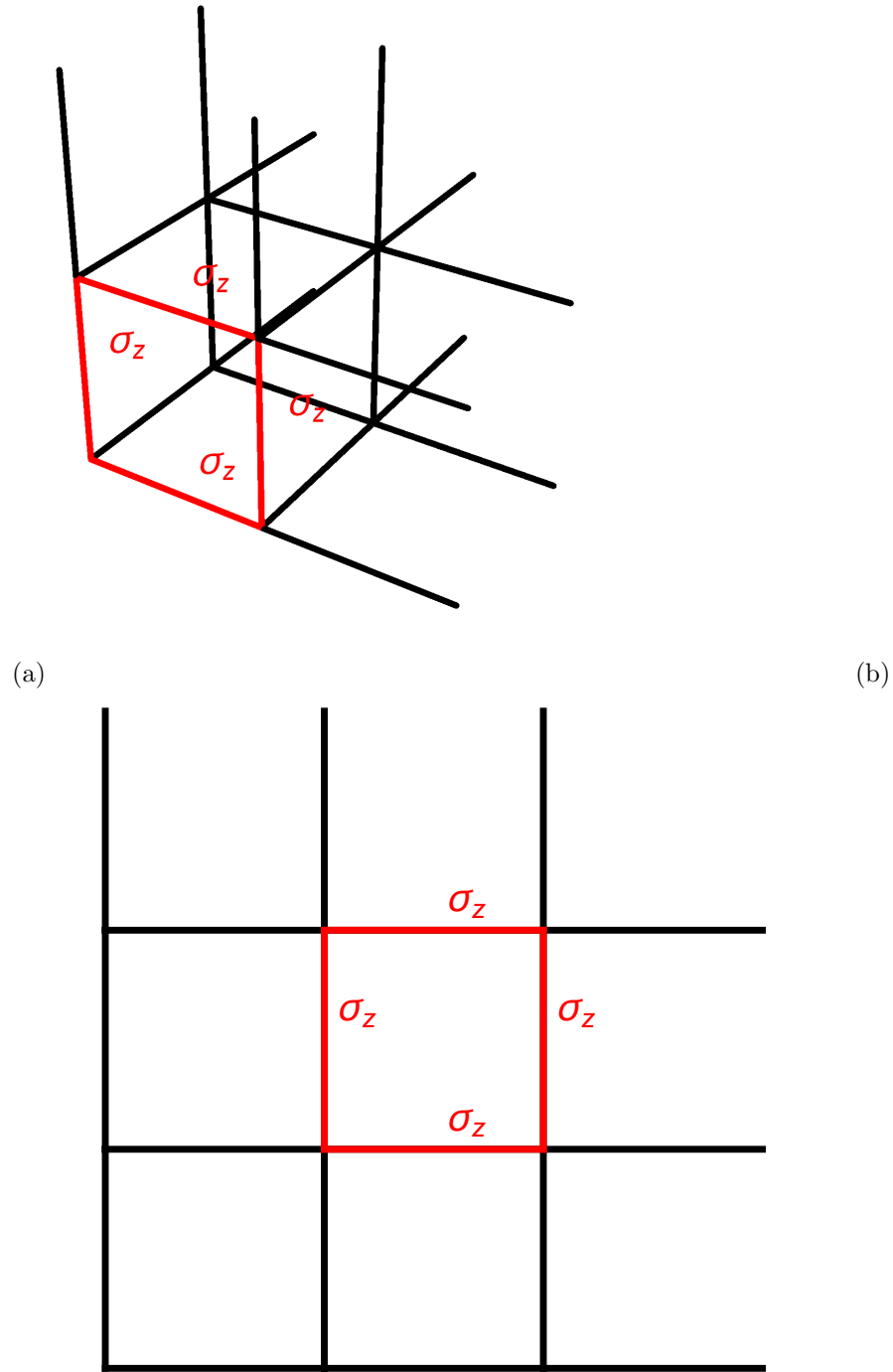


FIG. 1. (a)  $d=3$  and (b)  $d=2$  lattices, with an elementary plaquette indicated.

### B. Quantum Adiabatic algorithm and quantum circuit

In adiabatic evolution,  $g$  varies gradually, allowing the system to adapt to the instantaneous ground state. If the system starts as an eigenstate of the initial Hamiltonian  $Z$ , it

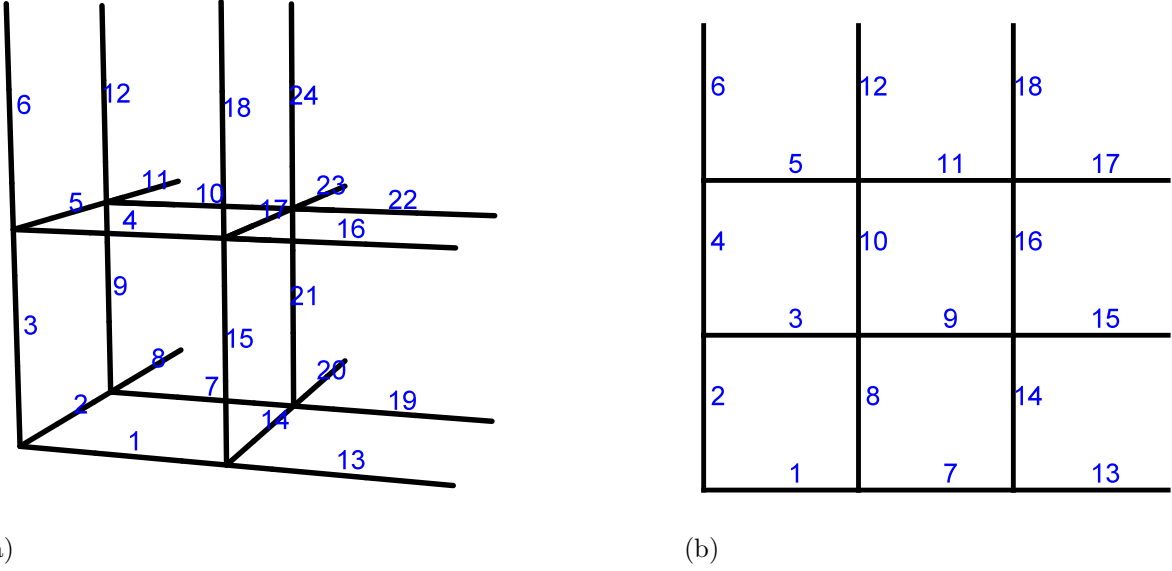


FIG. 2. (a)  $d=3$   $2 \times 2 \times 2$  lattice and (b)  $d=2$   $3 \times 3$  lattice, with ordering numbers of the links each occupied by a qubit. There are 24 qubits on the  $d=3$  lattice, while 18 qubits on the  $d=2$  lattice.

ends up as the corresponding eigenstate of the final Hamiltonian.

In our simulation, each time  $g$  is updated, the state evolves for a short time, as realized by quantum circuits. As  $H$  consists of two noncommutative parts  $Z$  and  $gX$ , it is decomposed by using Trotter decomposition. It is known that the evolution of time  $\tau$  under  $H_1 + \dots + H_q$  can be approximated as the consecutive evolution under  $H_1, \dots, H_q$  for  $m$  decompositions of time  $\tau/m$ , with the error [2]

$$\|e^{-i(H_1+\dots+H_q)\tau} - (e^{-iH_1\tau/m} \dots e^{-iH_q\tau/m})^m\| = O\left(\frac{ql\tau^2}{m}\right), \quad (4)$$

where  $l$  is the largest norm of the commutators of any two of these Hamiltonians.

In our problem, the decomposition is

$$e^{-iHt_s} \approx \left(\prod_{\square} e^{-iZ_{\square}t_s/n} e^{-igX_{\square}t_s/n}\right)^n, \quad (5)$$

where  $t_s$  is the time for each step in our  $g$  variation, while  $t_s/n$  is the time for each step in its Trotter decomposition, which is realized in terms of quantum circuit,

$$e^{-iZ_{\square}t_s/n} = AR_z^a(-2t_s/n)A, \quad A = \prod_{l \in \square} CNOT_{l,a}, \quad (6)$$

where the quantum gate  $R_z^a(\phi) \equiv e^{i\sigma_z^a\phi/2}$  on ancilla represents rotation of angle  $\phi$  around z-axis,  $CNOT_{l,a}$  is a CNOT gate controlled by the qubit  $l$  and targeting on the ancilla  $a$ ,

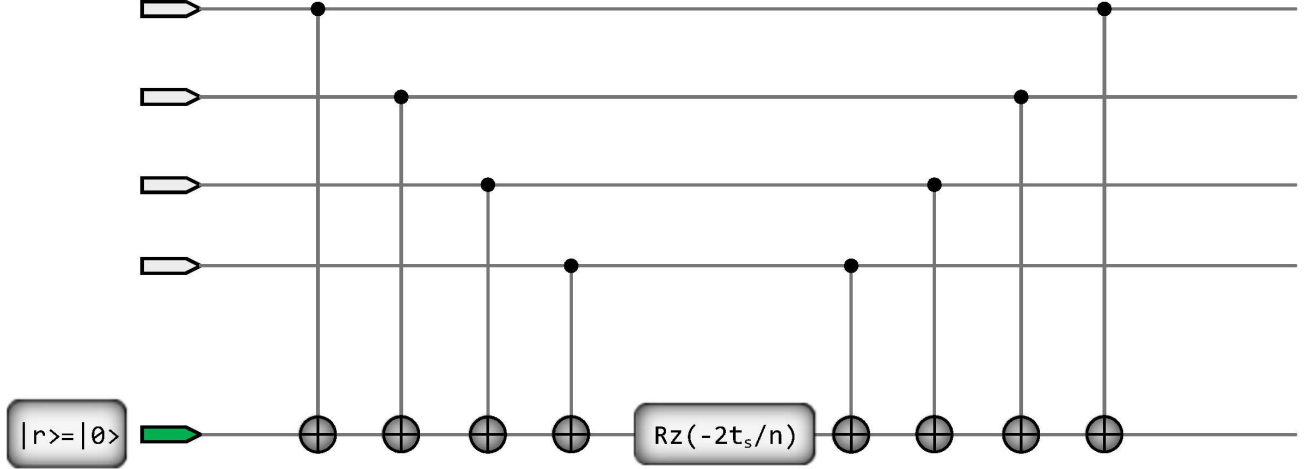


FIG. 3. The quantum circuit for  $e^{-iZ_{\square}t_s/n}$  or  $e^{iZ_{\square}t_s/n}$ , depending on whether the state of the ancilla is  $|0\rangle$  or  $|1\rangle$ .

as shown in Fig. 3. Initially, the ancilla is set to be  $|r\rangle = |0\rangle$ . Preceding  $R_z^a(-2t_s/n)$ , each CNOT flips  $|r\rangle$  if and only if the control qubit is  $|1\rangle$ . Therefore  $R_z^a(-2t_s/n)$  acts as  $e^{it_s/n}$  when there are even number of  $|1\rangle$ 's on the plaquette, and acts as  $e^{-it_s/n}$  when there are odd number of  $|1\rangle$ 's on the plaquette. This is precisely the effect of  $e^{-iZ_{\square}t_s/n}$ . Finally, the four CNOT gates after  $R_z^a(-2t_s/n)$  return  $|r\rangle$  to  $|0\rangle$ , which can be used for the next plaquette. If we set  $|r\rangle = |1\rangle$  initially, this circuit can be used to simulate an evolution of the reversed time  $-t_s/n$ .

For the other part  $gX$  in the Hamiltonian,

$$e^{-igXt_s/n} = \prod_l e^{-i(-\sigma_l^x)gt_s/n} = \prod_l R_x^l(2gt_s/n), \quad (7)$$

where  $R_x^l(\phi)$  on qubit  $l$  represents rotation of angle  $\phi$  around the x-axis.

### C. Initial Ground State

The adiabatic quantum simulation starts with  $g = 0$ , i.e.  $H = Z$ , of which there are many degenerate ground states satisfying

$$Z_{\square} = -1, \forall \square, \quad (8)$$

which is prepared through the quantum circuit in Fig. 4. For each plaquette, following the preparation of the equal superposition of all basis states using Hadamard gates, the CNOT

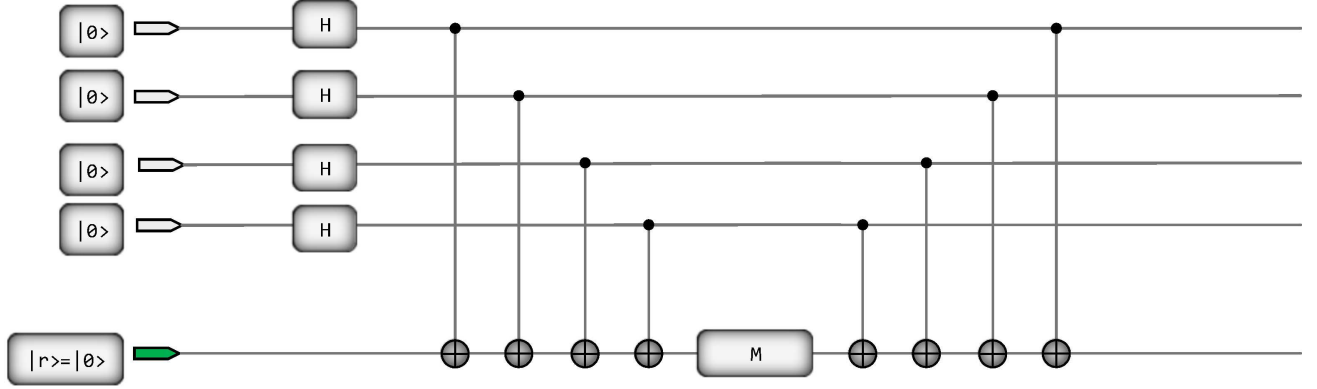


FIG. 4. The quantum circuit preparing the initial ground state of  $Z_{\square}$  for one elementary plaquette.

gates produce the state  $\frac{1}{\sqrt{2}}(|r=0\rangle_a |Z_{\square} = -1\rangle + |r=1\rangle |Z_{\square} = 1\rangle)$ , where the ancilla and the plaquette are entangled, with the equality between  $\sigma_z^a = 2r - 1$  and  $-Z_{\square}$  in each branch. Then the measurement operation  $M$  on the ancilla projects it to be in  $|r=0\rangle$ , thus selects the plaquette state to be  $|Z_{\square} = -1\rangle$ , which is the ground state for  $g = 0$ .

QuEST provides a method function of controlled collapse to the destined state, which is convenient for preparing the initial ground state in the simulator.

#### D. Adiabatic condition

The variation of  $g$  should be much slower than the dynamical time scale. To determine the dynamical time scale, we prepare the ground state for a certain value of  $g$ , through adiabatic evolution from the ground state for  $g = 0$ . In this ground state, the expectation values of  $Z$  and  $gX$  oscillate. As shown in Fig. 5, the order of magnitude of the oscillation period is 1. Therefore  $g$  can be varied from 0 to 2 for a time interval of the order of  $t = 10 \sim 100$ , which is much longer than the oscillation period.

Now we examine the error in Trotter decomposition given in Eq. (4). In the present problem,  $l = 1$ . For  $d=3$  lattice, the number of terms in the Hamiltonian is  $q = 24 + 24 = 48$ , and we choose the final value of  $g$  to be  $g_f = 2$ , and the total evolution time to be  $t_f = 30$ . For each step of  $g$  variation, the time is  $t_s = 0.01$ , the increase of  $g$  is  $g_s = 0.001$ , and the number of Trotter decompositions is  $n = 500$ . Thus the number of steps of  $g$  variation is  $N_s = g_f/g_s = t_f/t_s = 3000$ , and the total number of Trotter decompositions

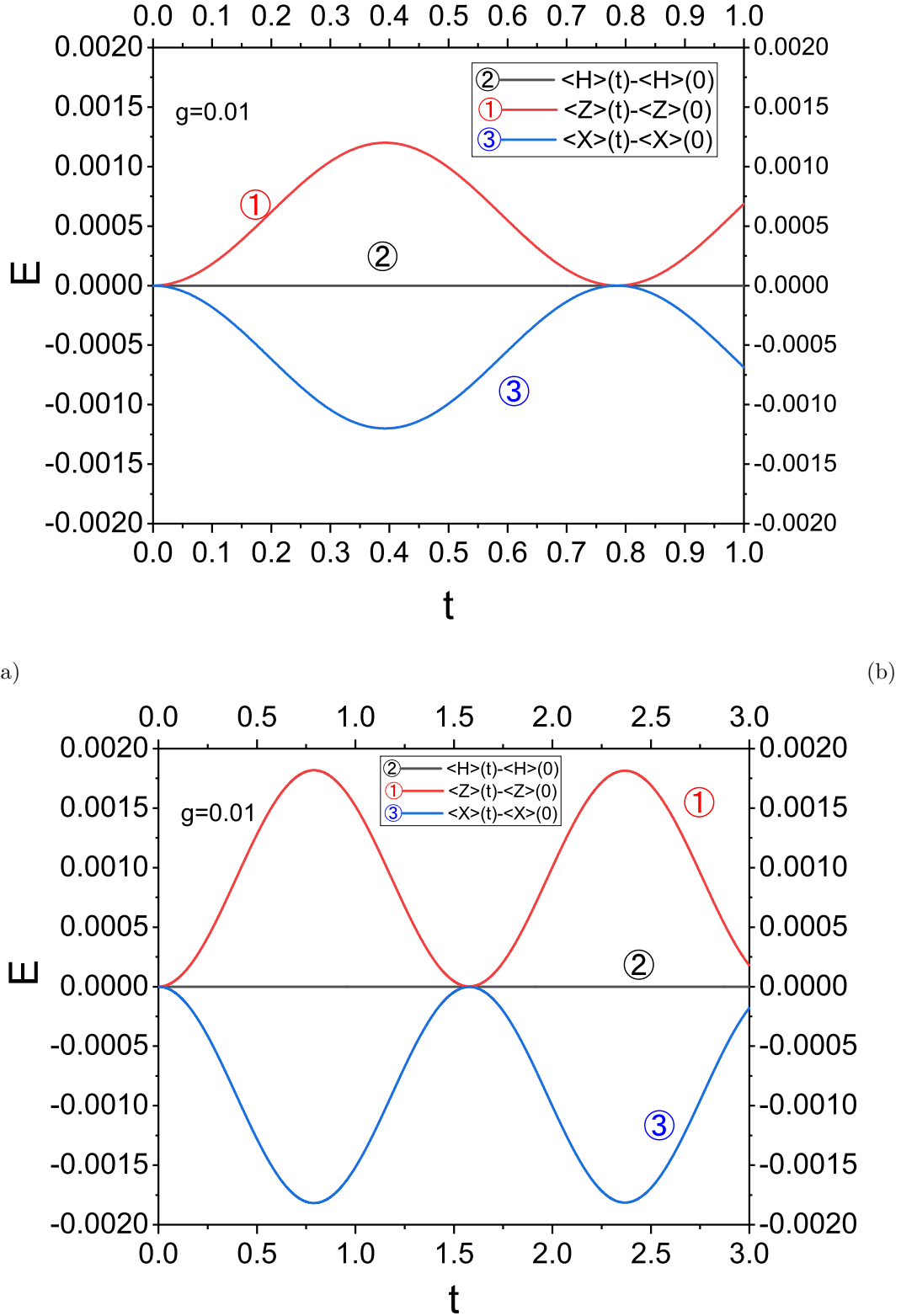


FIG. 5. In the ground state for  $g = 0.01$ , difference between the expectation values of  $H$ ,  $Z$  and  $gX$  at time  $t$  and those at time  $t = 0$ . (a)  $d=3$   $2 \times 2 \times 2$  lattice. (b)  $d=2$   $3 \times 3$  lattice.

is  $nN_s = 1500000$ , and the total error is 3.8%. For  $d=2$ ,  $q = 18 + 9 = 27$ , and we choose  $g_f = 3$ ,  $t_f = 60$ ,  $g_s = 0.001$ ,  $t_s = 0.02$ ,  $n = 5000$ . Thus  $N_s = 3000$ . The total number of Trotter decompositions is 15000000, and the total error is 0.86%.

These parameter values are chosen to allow the computation to be completed in an acceptable time under adiabatic condition. It turns out that the computation time is about one week, and the accuracy is acceptable.

The adiabatic condition constrains that the matrix element of  $\partial H/\partial t$  should be much smaller than the energy gap [33]. The former is of the order of  $\partial g/\partial t = g_s/t_s = 0.1$ . The energy gap can be estimated as the energy of creating a pair of visons, which is 4. Therefore, the adiabatic condition is indeed satisfied.

### E. Simulation of Measurement

The energy is the expectation value of  $H$ ,  $E = \langle H \rangle = \langle Z \rangle + g \langle X \rangle$ . In state  $|\psi\rangle$ ,  $E = \langle \psi | H | \psi \rangle = \sum_i E_i P(E_i)$ ,  $\langle Z \rangle = \langle \psi | Z | \psi \rangle = \sum_i z_i P(z_i)$ ,  $\langle X \rangle = \langle \psi | X | \psi \rangle = \sum_i x_i P(x_i)$ , where  $\{E_i\}$ ,  $\{z_i\}$  and  $\{x_i\}$  represent the measurement results of  $H$ ,  $Z$  and  $X$ , respectively,  $P(E_i)$ ,  $P(z_i)$  and  $P(x_i)$  are probability distributions, called densities of states below. In our classical simulator, we obtain  $E$  by summing up  $\langle Z \rangle$  and  $g \langle X \rangle$ .

We also calculate the expectation value of Wegner-Wilson loop operator

$$W_C = \prod_{l \in C} \sigma_l^z, \quad (9)$$

which is the product of  $\sigma_z$  on the links along any closed contour  $C$  on the direct square lattice, as shown in Fig. 1.

We use CUDA parallel acceleration method to count the statistical summation of all basis vectors on GPU. We write our own codes for the calculation of the measurement results, which are not included in QuEST. The measurement is simulated for every updated value of  $g$ . All these quantities can be calculated in terms of the distribution  $\{P(z_i)\}$  in the representation  $\{\sigma_l^z\}$ , as  $\langle Z \rangle = -\sum_{\square} \langle \psi | \prod_{l \in \square} \sigma_l^z | \psi \rangle$ ,  $\langle X \rangle = -\sum_l \langle \psi | \mathbb{H} \sigma_l^z \mathbb{H} | \psi \rangle$ , where  $\mathbb{H}$  is Hadamard gate,  $\langle W_C \rangle = \langle \psi | \prod_{l \in C} \sigma_l^z | \psi \rangle$ .

In real quantum simulation,  $E$  can also be obtained by using quantum phase estimation. For a fixed value of  $g$  in a short time period  $t_s$ ,  $e^{-iHt} |u\rangle = e^{-i\phi} |u\rangle$ , where  $\phi \equiv Et_s$ . Define

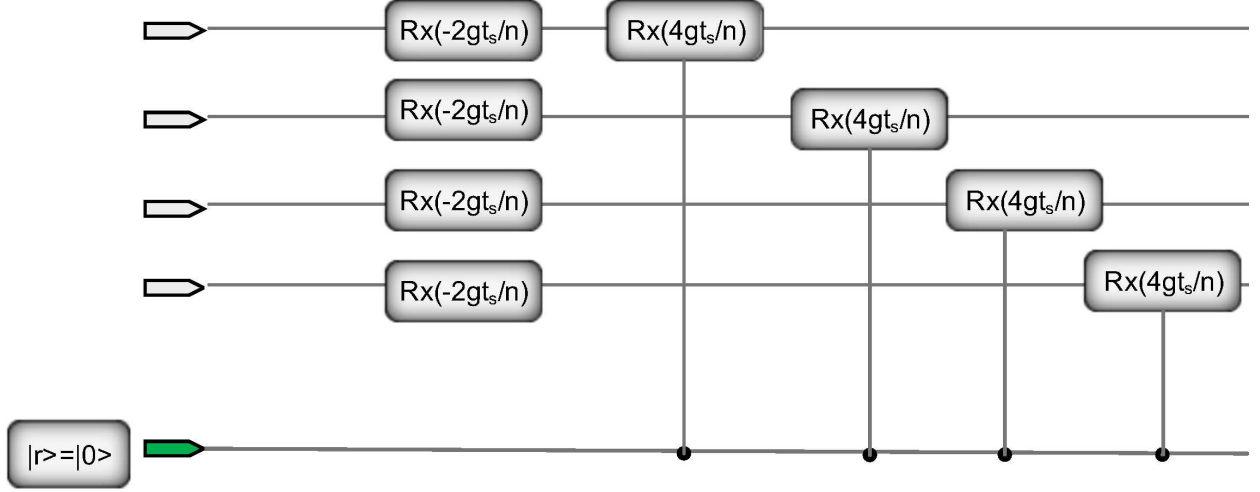


FIG. 6. The quantum circuit for  $\prod_{l \in \square} e^{i\sigma_l^x gt_s/n}$  or  $\prod_{l \in \square} e^{-i\sigma_l^x gt_s/n}$ , depending on whether the state of the ancilla is  $|0\rangle$  or  $|1\rangle$ .

the conditional evolution, controlled by an ancilla,

$$U(t) = |0\rangle \langle 0| \otimes e^{-iHt} + |1\rangle \langle 1| \otimes e^{iHt}, \quad (10)$$

which can be realized in terms of controlled gates. For  $Z$  part, the method is as shown in Fig. 3. For  $X$  part, the method is as shown in Fig. 6.

Then  $U(t) \frac{1}{\sqrt{2}}(|0\rangle + |1\rangle) |u\rangle = e^{-i\phi} \frac{1}{\sqrt{2}}(|0\rangle + |1\rangle e^{i2\phi}) |u\rangle$ . Therefore,  $U(2^n t) \frac{1}{\sqrt{2}}(|0\rangle + |1\rangle) |u\rangle = e^{-i2^n \phi} \frac{1}{\sqrt{2}}(|0\rangle + e^{i2^n \cdot 2\phi} |1\rangle) |u\rangle$ , ( $n = 0, 1, 2, \dots$ ). Hence the probability distribution of  $2\phi$ , and thus  $E$ , can be obtained by using phase estimation. One can use the ancilla to control the time direction.

## F. Hardware Platform

We use a Nvidia K40m GPU server, which was used by QuEST team in their simulation of 29 qubits with float decision [32]. We estimated the maximal scales of quantum simulations that QuEST can simulate under different precisions, as listed in Table.I. Among different precisions, we use double precision.

| Simulation Precision | $N_f$ | $N_{qubit}$ | $M$   |
|----------------------|-------|-------------|-------|
| float                | 4     | 30          | 8.2GB |
| double               | 8     | 29          | 8.2GB |
| long double          | 16    | 28          | 8.2GB |

TABLE I. Maximal scales that QuEST can perform with one Nvidia K40m GPU card.  $N_f$  is the byte number of a floating point number,  $N_{qubit}$  is the number of qubits,  $M$  is the memory requirement.

### III. SIMULATION RESULTS

#### A. Wegner-Wilson loop and QPT critical point

Now we turn to the results of our simulation for both  $D=3+1$  and  $D=2+1$ . We first prepare the initial ground state at  $g = 0$ , then execute the adiabatic algorithm by varying  $g$  from 0 to 2 in steps  $g_s = 0.001$ . At each step, several quantities are calculated.

As  $g$  increases, the state evolves from the one with all plaquettes in  $Z_{\square} = -1$  to the state with all qubits in  $\sigma^x = 1$ . During this process, it undergoes a QPT, which can be characterized in terms of the Wegner-Wilson loop  $W_C$  [19]. In the confined phase at  $g \gg 1$ ,  $W_C$  obeys the area law  $\langle W_C \rangle \sim \exp(-\alpha A_C)$ , where  $A_C$  is the area enclosed by the contour  $C$ ,  $\alpha$  is a constant. In the deconfined phase at  $g \ll 1$ ,  $W_C$  obeys the perimeter law  $\langle W_C \rangle \sim \exp(-\alpha' P_C)$ , where  $P_C$  is the perimeter of the contour  $C$ ,  $\alpha'$  is a constant. At  $g = 0$ , all  $Z_{\square} = -1$ , the  $\mathbb{Z}_2$  flux is expelled, the small fluctuations leads to the perimeter law.

Our simulation confirms that with the increase of  $g$ ,  $W_C$  changes from the perimeter law to the area law in passing the phase transitions. For both  $d=3$  and  $d=2$  lattices, we choose three contours  $C1$ ,  $C2$ ,  $C3$ , as shown in Fig. 7. Their perimeter ratio is 1:1.5:2 while their area ratio is 1:2:3. The simulation results show that  $\langle W_C \rangle$  of the three loops indeed agree with the two laws, as shown in Fig. 8.

We have also determined the critical parameter  $g_c$  of the QPT. In each step of adiabatic evolution, we calculate  $\langle Z \rangle$  and  $\langle X \rangle$ , which are summed to give  $\langle H \rangle$ , as shown in Fig.9, from which we also obtain the first and second order derivatives with respect to  $g$ , as shown in

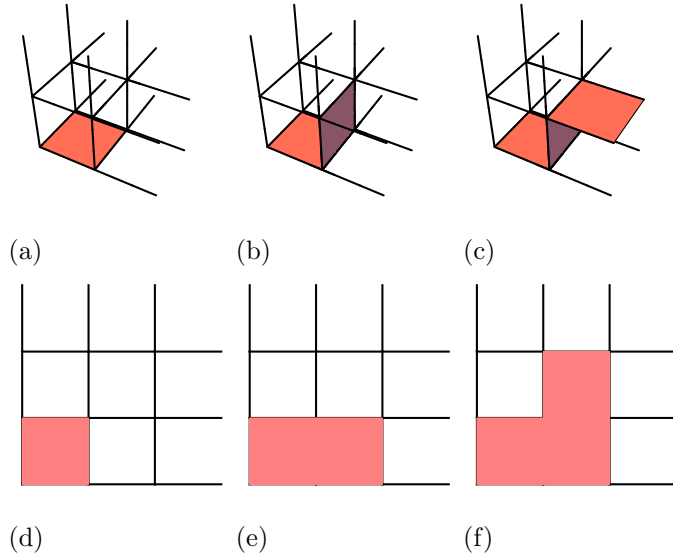


FIG. 7. (a-c) Three Wilson loop contours on d=3 lattice. (d-f) Three Wilson loop contours on d=2 lattice.

Fig.10. From the crossing point of  $\langle Z \rangle$  and  $g\langle X \rangle$ , and from the peak of the derivatives, it is determined that

$$g_c \approx 1.03, \quad D = 3 + 1, \quad (11)$$

$$g_c \approx 0.40, \quad D = 2 + 1, \quad (12)$$

which is consistent with previous result implied from duality.  $D = 3 + 1$  theory is self-dual, hence  $g_c = 1$  [16, 34].  $D=2+1$  theory is dual to  $D=2+1$  transverse Ising model, whose critical parameter is  $\lambda_c \approx 2.742 \sim 3.046$  [16, 17, 35], which implies  $g_c = 1/\lambda_c \approx 0.36 \sim 0.33$ .

### B. Forbidden bands in the densities of states

First consider d=3  $2 \times 2 \times 2$  lattice, with periodic boundary condition. The possible eigenvalues of  $Z$  are  $-24, -16, -12, \dots, 16, 24$ , while the possible eigenvalues of  $X$  are  $-24, -22, \dots, 24$ , for the following reasons. As shown in Fig. 11, flipping one qubit between  $\sigma_z$  eigenstates changes the signs of the eigenvalues of  $Z_{\square}$ 's of 4 plaquettes sharing this qubit, and thus changes the eigenvalue of  $Z$  by 8; flipping two neighboring qubits between  $\sigma_z$  eigenstates changes the signs of the eigenvalues of  $Z_{\square}$ 's of 6 plaquettes sharing this qubit, and thus changes the eigenvalue of  $Z$  by 12; in general,  $4 + 2n$  plaquettes can be excited

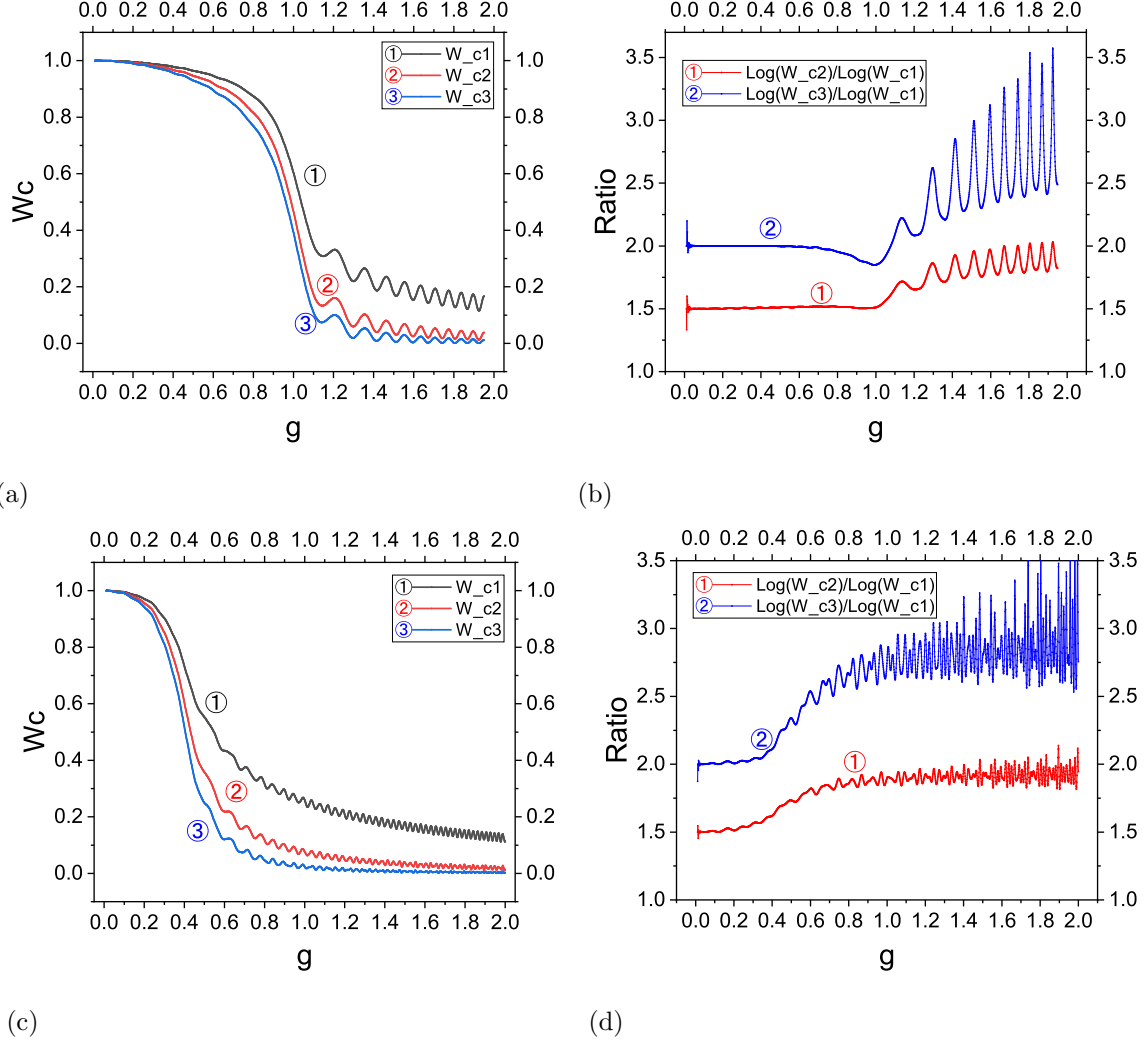


FIG. 8. Expectation values of three Wegner-Wilson loops as functions of  $g$ . The results are obtained in each step of increasing  $g$  by  $g_s = 0.001$ . (a) Results for  $d=3$   $2 \times 2 \times 2$  lattice. (b) Two ratios between logarithms of the expectation values in (a). (c) Results for  $d=2$   $3 \times 3$  lattice. (d) Two ratios between logarithms of the expectation values in (c).

( $n = 0, 1, 2, \dots$ ). Flipping one qubit between  $\sigma_x$  eigenstates changes the eigenvalue of  $X$  by 2. There are several forbidden bands in DOS' of  $Z$  and  $X$ , where the DOS' vanish.

Moreover,  $D=3+1$  quantum  $Z_2$  theory is self-dual, hence DOS of  $Z$  and DOS of  $X$  exhibit significantly similar characteristics, with opposite tendencies with respect to  $g$ , as shown in Fig. 12 and Fig. 13. As derived from DOS' of  $Z$  and  $X$ , with the increase of  $g$  from 0, the expectation value of  $Z$  increases from  $-24$  towards 0, and while the expectation value of  $X$  decreases from 0 to  $-24$  (Fig 9).

In  $d=2$ , there is no forbidden band in DOS of  $Z$ , as it is possible to excite only 2 visons

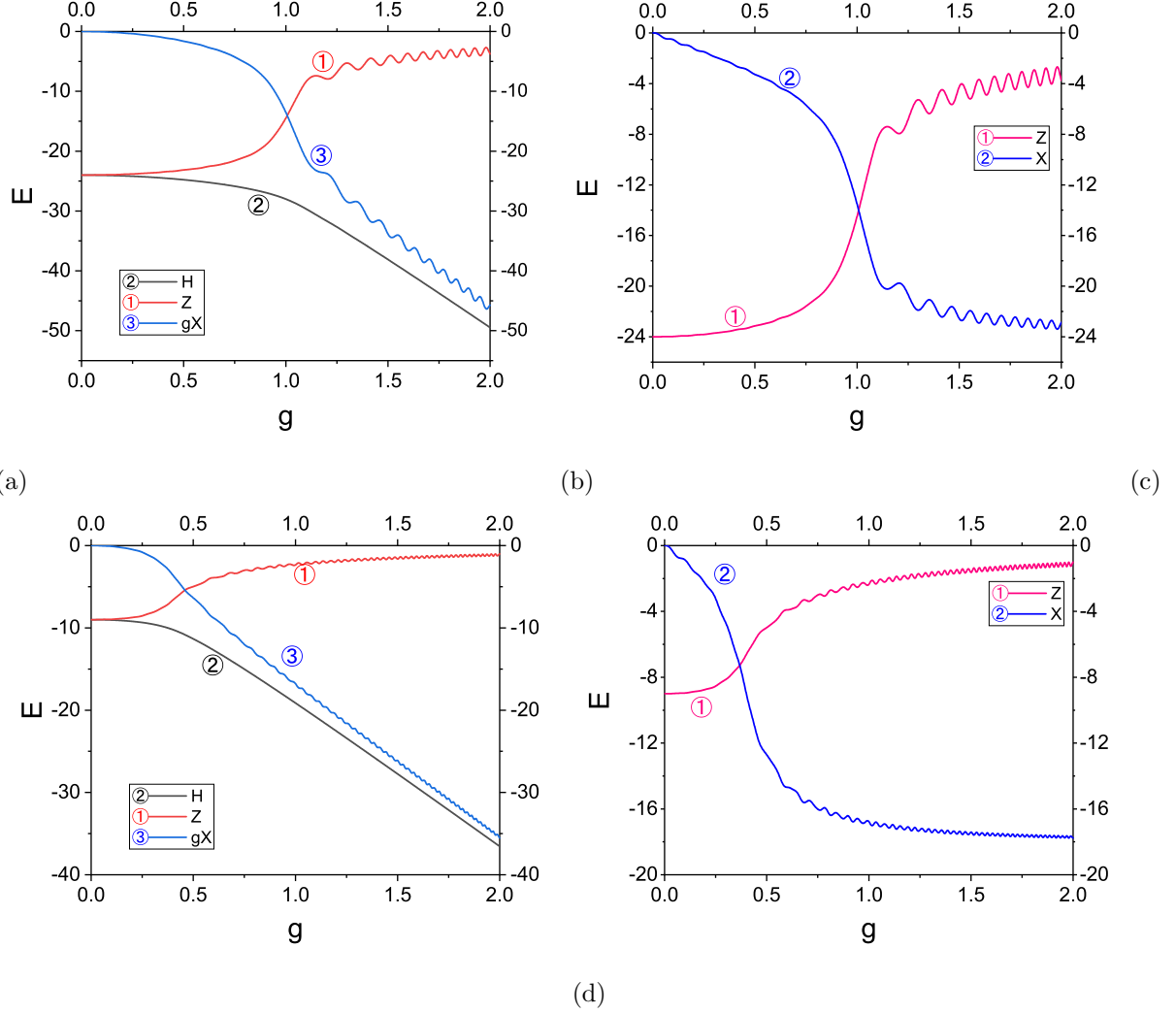


FIG. 9.  $\langle Z \rangle$ ,  $\langle X \rangle$ ,  $g\langle X \rangle$  and  $\langle H \rangle$  as functions of  $g$ , which varies from 0 to 2, in steps of  $g_s = 0.001$ . (a)  $\langle Z \rangle$ ,  $g\langle X \rangle$  and  $\langle H \rangle$  on  $d=3$   $2 \times 2 \times 2$  lattice.  $\langle Z \rangle$  and  $g\langle X \rangle$  cross at  $g_c \approx 1.03$ . (b)  $\langle Z \rangle$  and  $\langle X \rangle$  on  $d=3$   $2 \times 2 \times 2$  lattice, which clearly display self-duality. (c)  $\langle Z \rangle$ ,  $g\langle X \rangle$  and  $\langle H \rangle$  on  $d=2$   $3 \times 3$  lattice.  $\langle Z \rangle$  and  $g\langle X \rangle$  cross at at  $g_c \approx 0.40$  in  $d=2$ . (d)  $\langle Z \rangle$  and  $\langle X \rangle$  on  $d=2$   $3 \times 3$  lattice.

in  $d=2$  lattice, and the number of excited plaquettes is  $2 + 2n$ , ( $n = 0, 1, 2, \dots$ ), as shown in Fig.11. In  $d=2$   $3 \times 3$  lattice with periodic boundary condition, the possible eigenvalues of  $Z$  are  $-9, -5, \dots, 7$ , while the possible eigenvalues of  $X$  are  $-18, -16, \dots, 16, 18$ . However, while there is no forbidden band in DOS of  $Z$ , there are several forbidden bands in DOS of  $X$  (Fig. 12), in consistency with the fact that  $D=2+1$  theory is not self-dual. With the increase of  $g$  from 0, the expectation value of  $Z$  starts with  $-9$  and moves towards 0, while the expectation value of  $X$  starts with 0 and moves towards  $-18$ .

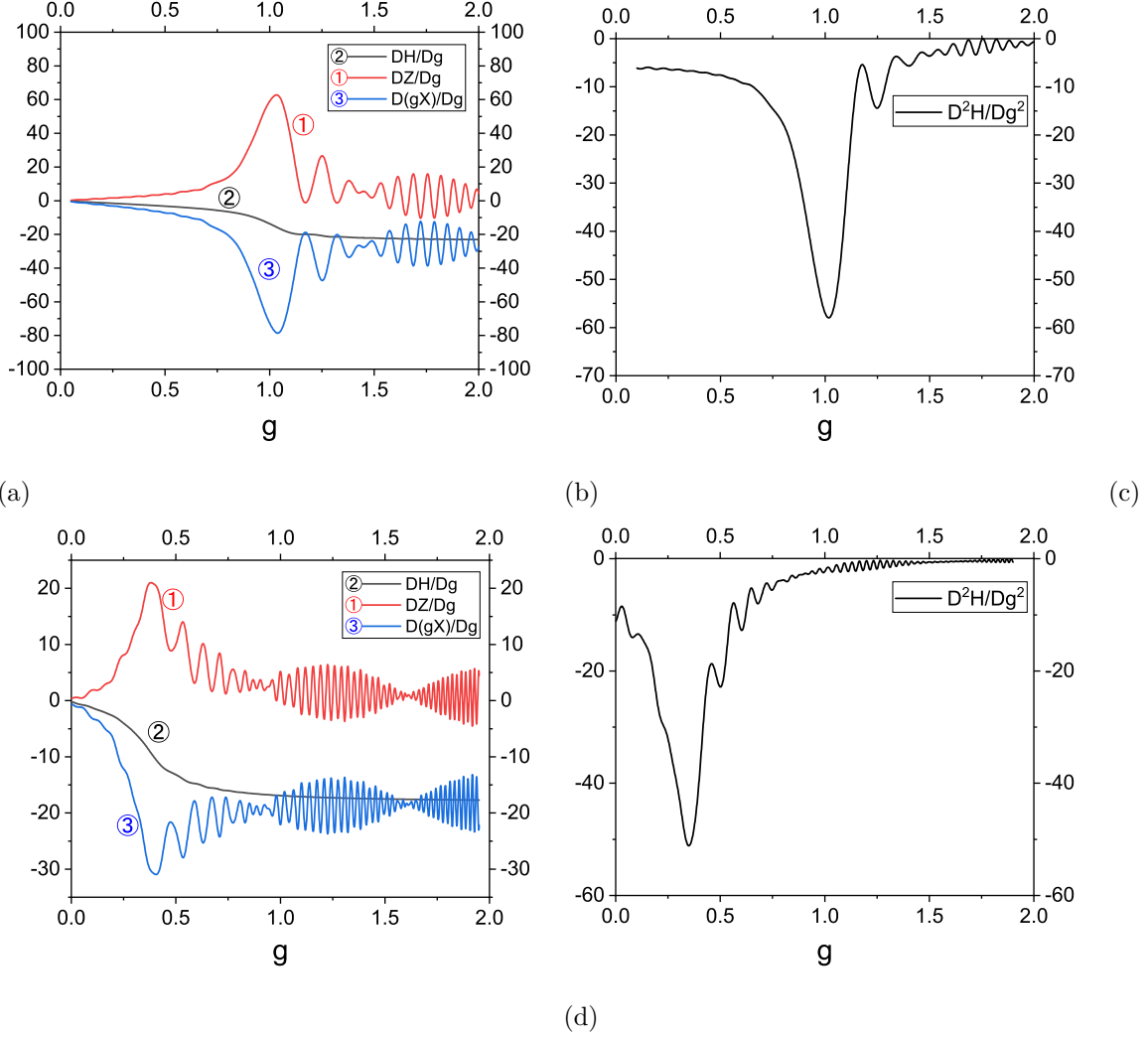


FIG. 10. Derivatives with respect to  $g$ , as functions of  $g$ , which varies from 0 to 2, in steps of  $g_s = 0.001$ . (a) First-order derivatives of  $\langle Z \rangle$ ,  $g\langle X \rangle$  and  $\langle H \rangle$  on d=3  $2 \times 2 \times 2$  lattice. (b) Second-order derivative of  $\langle H \rangle$  on d=3  $2 \times 2 \times 2$  lattice, the lowest valley is at  $g_c \approx 1.03$ . (c) First-order derivatives of  $\langle Z \rangle$ ,  $g\langle X \rangle$  and  $\langle H \rangle$  on d=2  $3 \times 3$  lattice. (d) Second-order derivative of  $\langle H \rangle$  on d=2  $3 \times 3$  lattice, the lowest valley is at  $g_c \approx 0.40$ .

### C. Order of QPT

Whether there exists first-order QPT is an interesting issue, as it may lead to quantum critical fluctuations dominating the low lying excitations [28]. The thermal phase transition in the classical  $\mathbb{Z}_2$  gauge theory is second-order in d=3, and is first-order in d=4 [27], implying that QPT is second-order in  $D=2+1$ , and is first-order in  $D=3+1$ . This is confirmed in our simulation.

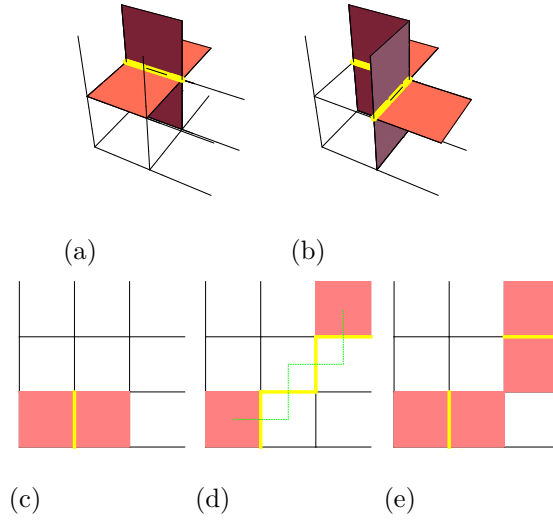


FIG. 11. Yellow link represents flipping the eigenstate of  $\sigma_z$ , pink  $\square$  means  $Z_{\square} = 1$ . (a)  $d=3$  lattice with one qubit flipped, and thus 4 plaquettes excited. (b)  $d=3$  lattice with two neighboring qubits flipped, and thus 6 plaquettes excited. If the qubits on two parallel neighboring links are flipped, then 4 plaquettes are excited. (c)  $d=2$  lattice with one qubit flipped, and thus 2 plaquettes excited. (d)  $d=2$  lattice with 2 separated visons created a string of  $\sigma_x$  operators. (e)  $d=2$  lattice with 2 qubits on different plaquettes flipped, and thus 4 plaquettes excited.

Our results demonstrate that QPT in  $\mathbb{Z}_2$  quantum gauge theory is second-order in  $D=2+1$ , and is first-order in  $D=3+1$ , for the following three reasons. First, as shown in Fig.13, in  $D=3+1$ , DOS of  $Z$  appears significantly different before and after QPT, with the peak shifted from a position less than  $-12$  to that larger than  $-12$ , while at the critical point  $g_c = 1$ , both peaks exist, indicating phase coexistence, a hallmark of first-order phase transition. Moreover, there exists a pseudogap at  $Z = -12$ . In  $D=2+1$ , in contrast, DOS of  $Z$  does not show clear change before and after the phase transition.

Second, it can be observed in Fig.9 that in  $D=3+1$ , the slope, i.e. the derivative of the energy with respect to  $g$ , changes discontinuously at  $g_c \approx 1$ , while in  $D=2+1$ , nowhere does the slope change discontinuously.

Third, as shown in Fig. 8, in  $D=3+1$ , the expectation values of Wegner-Wilson loops exhibit discontinuous changes in the slopes at  $g_c \approx 1$ , while there are only continuous changes in  $D=2+1$ . Moreover, in  $D=3+1$ , an overheating-like phenomenon can be seen in Fig. 8(b) that when  $g$  becomes smaller than  $g_c$ , there is a small regime in which the ratio of the expectation values increases with the decrease of  $g$ .

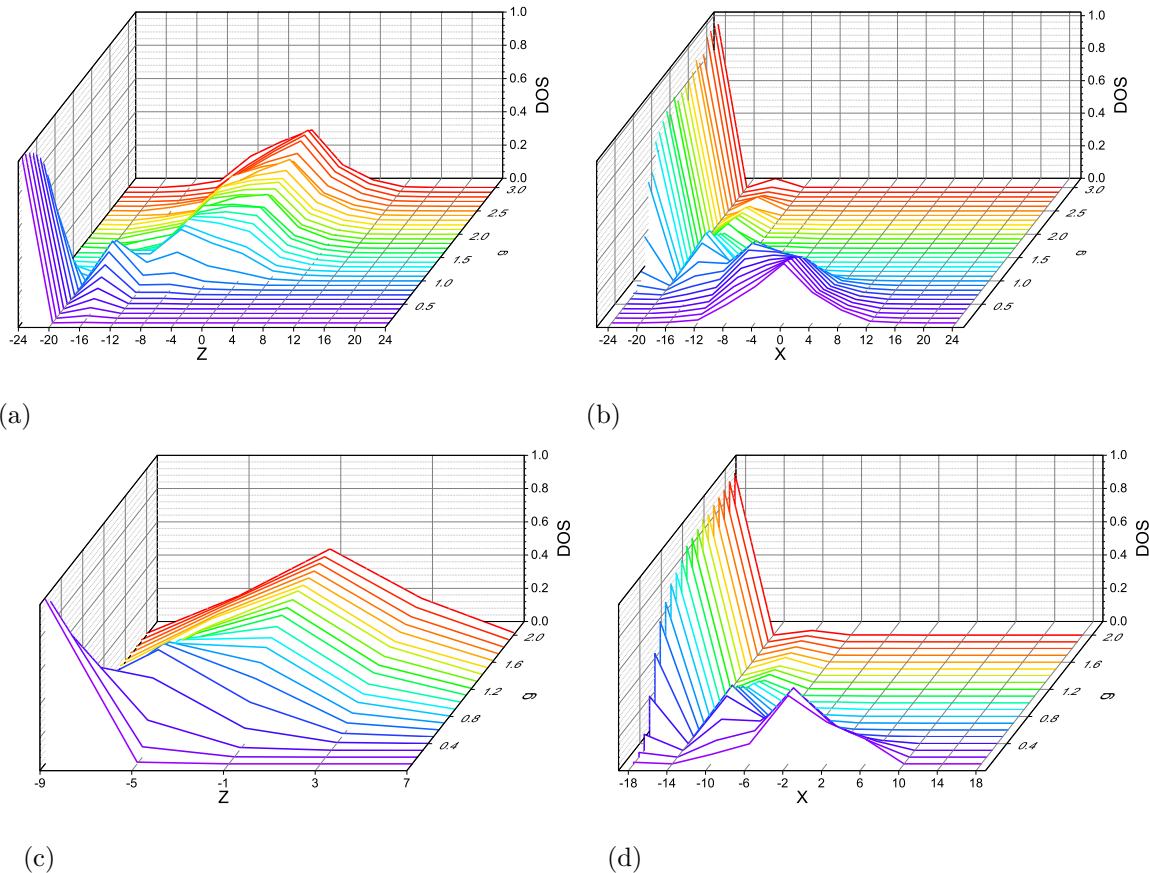


FIG. 12. DOS of  $Z$  or  $X$  as a function of the eigenvalues  $z$  or  $x$ , and  $g$ , which varies from 0 to 2, in steps of  $g_s = 0.001$ . (a)  $d=3$   $2 \times 2 \times 2$  lattice, DOS of  $Z$ . (b)  $d=3$   $2 \times 2 \times 2$  lattice, DOS of  $X$ . (c)  $d=2$   $3 \times 3$  lattice, DOS of  $Z$ . (d)  $d=2$   $3 \times 3$  lattice, DOS of  $X$ .

Moreover, we have also drawn together  $\langle Z \rangle$  and the second derivative of the energy with respect to  $g$  for  $d=2$  and  $d=3$  lattices, as shown in Fig. 14. It can be seen clearly that the change of  $\langle Z \rangle$  at QPT is much steeper in  $d=3$ , and that the valley in  $d=3$  is much sharper than in  $d=2$ . This suggests that QPT is first-order in  $D=3+1$  while second-order in  $D=2+1$ .

#### D. Topological QPT

Our simulation also verifies that QPT in quantum  $Z_2$  theory is topological, in three perspectives.

First, the absence of local symmetry breaking is verified in  $\langle \sigma_z \rangle$  of a single qubit as a function of  $g$ . As can be seen in Fig.15,  $\langle \sigma_z \rangle$  remains consistent with 0 for all values of  $g$ . We have also studied the average energy per link  $l$ ,  $\langle h_l \rangle$ , with  $h_l = z_l + x_l$ , where

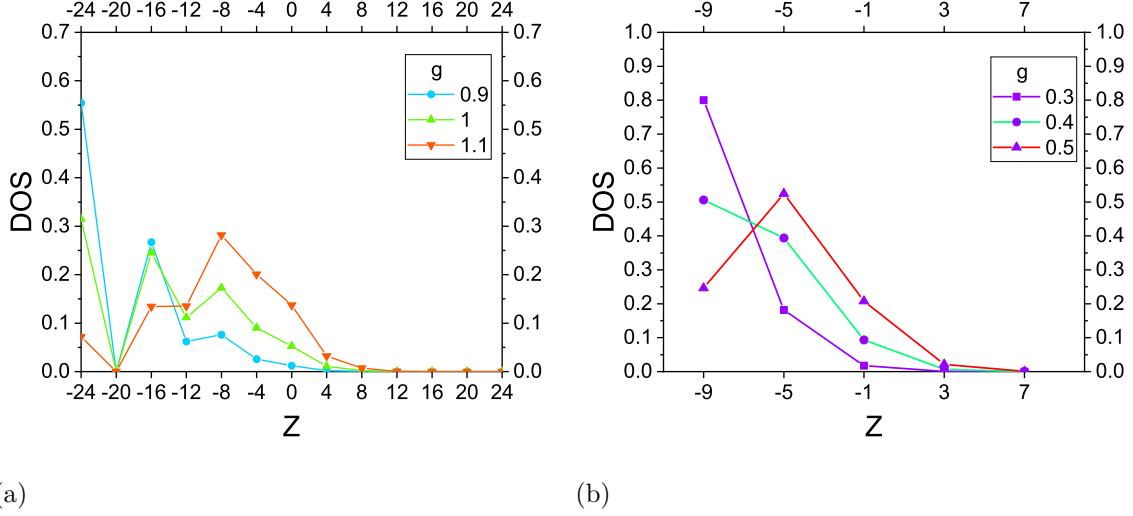


FIG. 13. DOS of  $Z$ . (a)  $d=3$   $2 \times 2 \times 2$  lattice,  $g = 0.9, 1.0, 1.1$ . (b)  $d=2$   $3 \times 3$  lattice,  $g = 0.3, 0.4, 0.5$ .

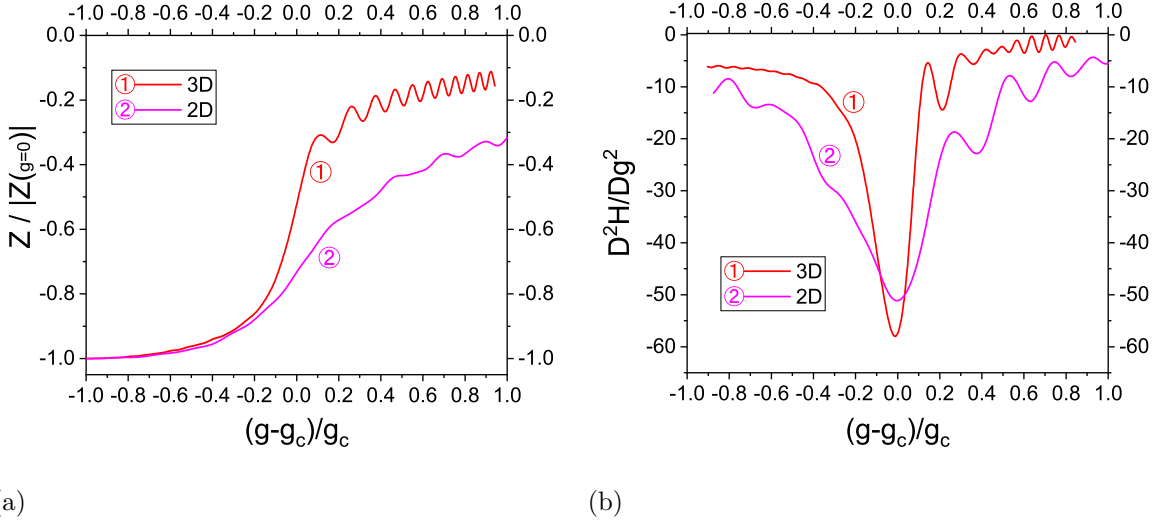


FIG. 14. Comparison of results for  $d=3$   $2 \times 2 \times 2$  and  $d=2$   $3 \times 3$  lattices, as functions of  $(g - g_c)/g_c$ , where  $g_c$  is the respective critical value in each dimensionality. (a)  $\langle Z \rangle$ , relative to the absolute value at  $g = 0$ . (b) Second derivative of the energy with respect to  $g$ . It can be seen clearly that in  $d=3$ , the change of  $\langle Z \rangle$  at QPT is much steeper, and the valley of second derivative of the energy is much sharper.

$$z_l = \frac{1}{N} \sum_{i=1, l \in \square_i}^N Z_{\square_i}, \quad x_l = -\sigma_l^x.$$

Second, the topological nature of QPT in  $D=2+1$  is also indicated by the stable low-lying excitations in the topological phase, called visons (Fig.12). As depicted in Fig.11, each vison carries  $\mathbb{Z}_2$  flux of  $-1$  [19], but cannot be created by any local operator acting on the ground state. Instead, one link excitation creates two visons, which can be separated by a string of

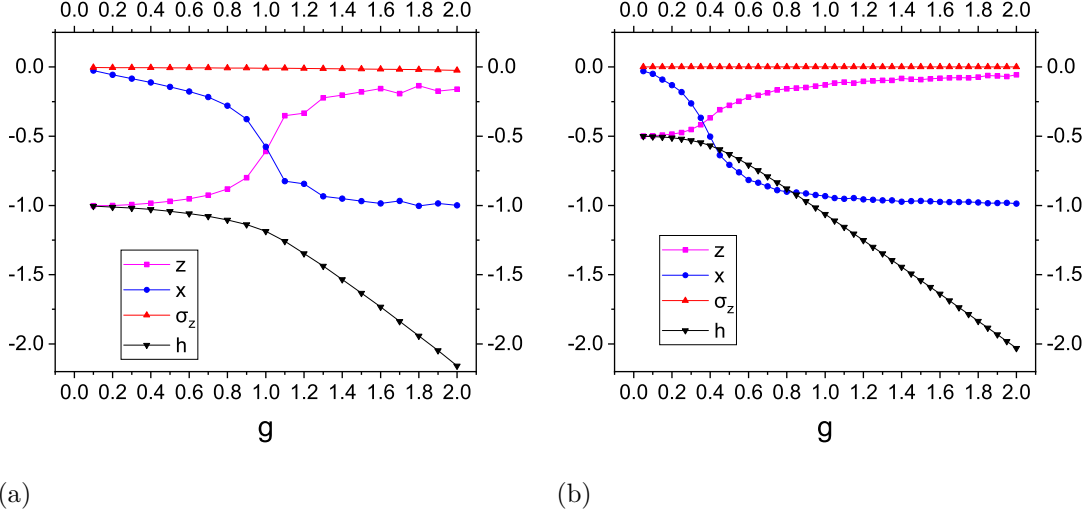


FIG. 15.  $\langle \sigma_z \rangle$ ,  $\langle z \rangle$ ,  $\langle x \rangle$  and  $\langle h \rangle$  of each link as functions of  $g$ . (a)  $d=3$   $2 \times 2 \times 2$  lattice,  $g$  increases by 0.1 in each step. (b)  $d=2$   $3 \times 3$  lattice,  $g$  increases by  $0.05$   $i/n$  each step.

$\sigma_x$  operators. The two separated visons can only be annihilated by a nonlocal operator or by contacting each other.

Yet another topological characteristic is the low-lying states on a topologically non-trivial geometry such as torus, with energy gap exponentially depending on  $g$  [19]. In  $D=d+1$ , one can define  $d$  independent operators commuting with  $H$ ,  $V_i \equiv \prod_{\bar{C}_i} \sigma_i$ , on contours  $\bar{C}_i$ , ( $i = 1, \dots, d$ ) as illustrated in Fig.16. In  $D=2+1$ ,  $\bar{C}_x$  and  $\bar{C}_y$  reside on the dual square lattice, and encircle the two independent cycles of the torus, In  $D=3+1$ ,  $\bar{C}_x$ ,  $\bar{C}_y$  and  $\bar{C}_z$  contain the links cut by the cross section.

As shown in Fig.16, one can also define Wegner-Wilson loop operators  $W_x = \prod_{C_x} \sigma_z$ ,  $W_y = \prod_{C_y} \sigma_z$ ,  $W_z = \prod_{C_z} \sigma_z$  on the direct lattice contours  $C_x$ ,  $C_y$  and  $C_z$ , which do not commute with  $H$ . There are the following commutation relations with  $V_i$ ,

$$W_x V_y = -V_y W_x, \quad W_y V_x = -V_x W_y. \quad (13)$$

Consequently  $W_x$  ( $W_y$ ) acting on an eigenstate of  $V_y$  ( $V_x$ ) yields an eigenstate with the opposite sign of the eigenvalue.

In  $D=2+1$ , at  $g = 0$ , there are 4 degenerate ground states with  $V_x = \pm 1$  and  $V_y = \pm 1$ . When  $g \neq 0$ , these 4 states are no longer degenerate, with the one with  $V_x = +1$  and  $V_y = +1$  being the ground state, while the three other states with exponentially small gaps

$$\Delta_{i1} \equiv E_i - E_1 \propto g^{L+1}, \quad (14)$$

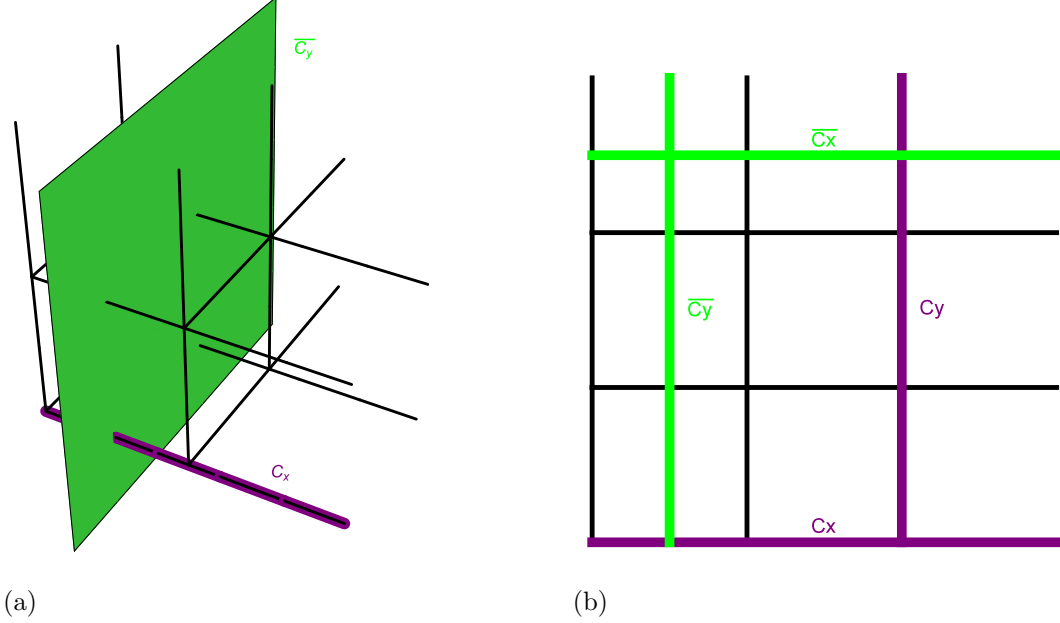


FIG. 16. (a) d=3 Lattice, with a contour  $\overline{C}_y$  in defining  $V_y$ , and a contour  $C_x$  in defining  $W_x$ . (b) d=2 Lattice, with contours  $\overline{C}_x$   $\overline{C}_y$  in defining  $V_x$  and  $V_y$  respectively, and contours  $C_x$  and  $C_y$  in defining  $W_x$  and  $W_y$  respectively.

where the subscript  $i = 2, 3, 4$  represents the three other states, while 1 refers to the ground state,  $L$  is the length of the torus. This is a defining characteristics of  $\mathbb{Z}_2$  topological order in  $D = 2 + 1$  [19]. We first prepare the four ground states at  $g = 0$  using  $W$  operators, then we simulate the quantum adiabatic algorithm on each ground state. As shown in Fig.17, we confirm that the energy gaps before the phase transition indeed satisfy Eq. (14).

In  $D=3+1$ , at  $g = 0$ , there are 8 degenerate ground states with  $V_x = \pm 1$ ,  $V_y = \pm 1$  and  $V_z = \pm 1$ . We prepare the ground state  $V_x = +1, V_y = +1, V_z = +1$  and the one with  $V_x = -1, V_y = -1, V_z = +1$  using the corresponding  $W$  operators. Then we execute adiabatic algorithm to obtain the dependence of energies and the gap on  $g$  before and after the phase transition, as shown in Fig. 17. A theory for this result at  $D=3+1$  is yet to be developed.

#### IV. SUMMARY

Using adiabatic quantum algorithm implemented in terms of quantum circuit, we design a scheme of quantum simulation of quantum  $\mathbb{Z}_2$  gauge theory, which is important in both

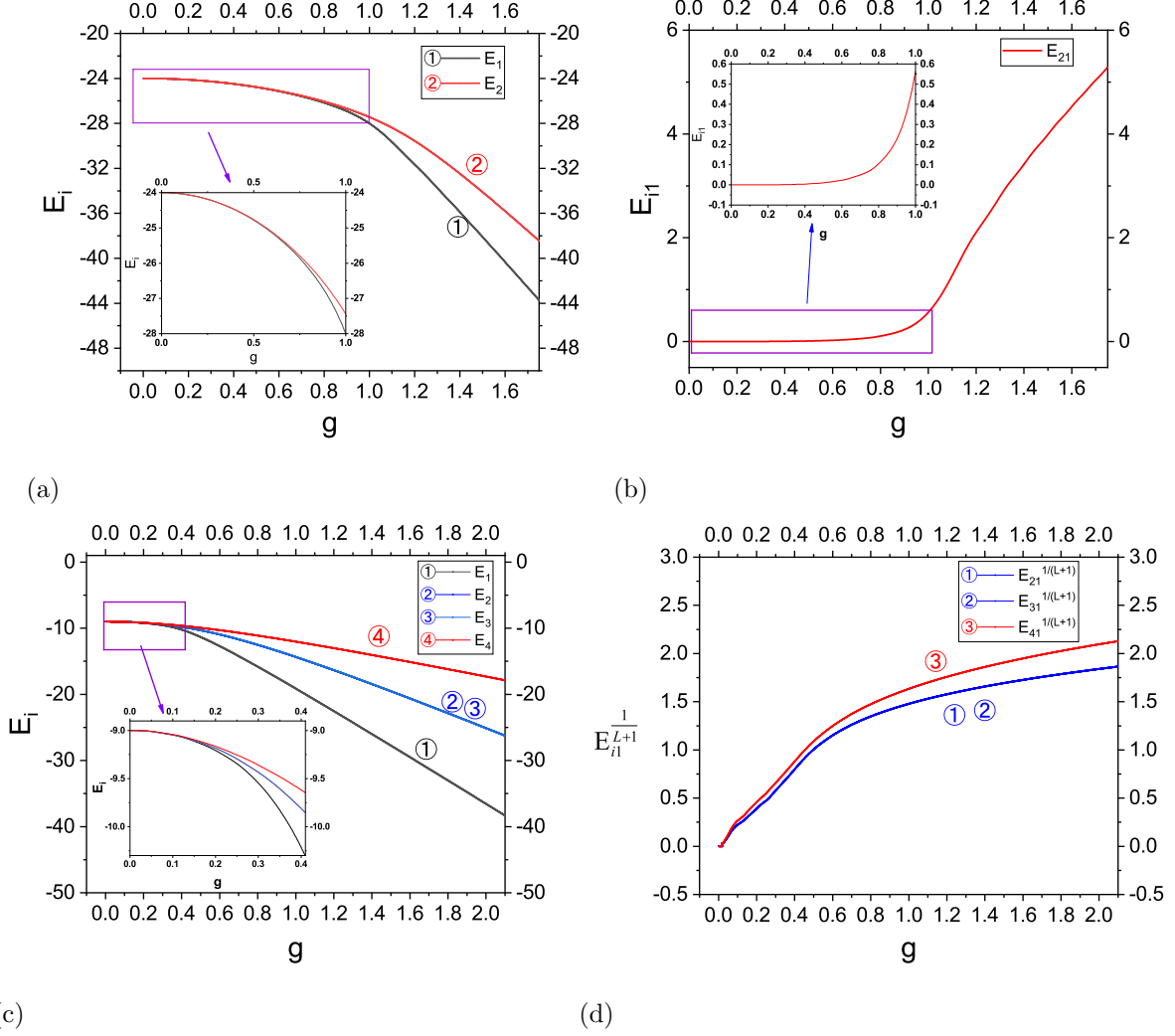


FIG. 17. (a) On  $d = 3 \ 2 \times 2 \times 2$  lattice, the energy eigenvalues  $E_1$  of the ground state, with  $(V_x, V_y) = (1, 1)$ , and  $E_2$  of the state with  $(V_x, V_y) = (1, -1)$ , as functions of  $g$ , which varies from 0 to 2, increasing by  $g_{step} = 0.001$  in each step. (b) On  $d = 3 \ 2 \times 2 \times 2$  lattice,  $E_{21} \equiv E_2 - E_1$  as a function of  $g$ . (c) On  $d = 2 \ 3 \times 3$  lattice, the energy eigenvalues  $E_1$  of the state with  $(V_x, V_y) = (1, 1)$ ,  $E_2$  of the state with  $(V_x, V_y) = (1, -1)$ ,  $E_3$  of the state with  $(V_x, V_y) = (1, -1)$ , and  $E_4$  of the state with  $(V_x, V_y) = (-1, -1)$ .  $g$  varies from 0 to 2, increasing by  $g_{step} = 0.001$  in each step. (d) On  $d = 2 \ 3 \times 3$  lattice,  $\Delta_{i1}^{-1/(L+1)}$ , ( $i = 2, 3, 4$ ), as functions of  $g$ , where the gap  $\Delta_{i1} \equiv E_i - E_1$ .

high energy physics and condensed matter physics. Especially, we classically simulate this quantum simulation by running the GPU simulator QuEST on a Nvidia K40m GPU server.

We have studied both  $D=2+1$  and  $D=3+1$  quantum  $\mathbb{Z}_2$  gauge theories. QPT is observed and determined to be first-order in  $D=3+1$  and second order in  $D=2+1$ , with critical point  $g_c$  is determined to be 1.03 and 0.40 respectively. Furthermore, we clearly observe the

topological characteristics of QPT, including the absence of local symmetry breaking, as well as the visons and the gaps exponentially dependent on  $g$  in  $D=2+1$ .

As demonstrated in this work, high-performance classical simulation of quantum simulation, which may be dubbed pseudoquantum simulation, represents a new way of computation, in addition to facilitating the development of quantum software. As the next step towards quantum simulation of lattice gauge theory, we shall study Fermions coupled with the gauge field using our method.

## ACKNOWLEDGMENTS

We would like to thank supercomputing center of USTC for their support, and the authors of QuEST for their GPU simulator and development documentation. This work was supported by National Science Foundation of China (Grant No. 11574054).

- 
- [1] Lloyd, S. Universal quantum simulators. *Science* **273**,
  - [2] Childs, A. M. *et al.* Exponential algorithmic speedup by quantum walk. *eprint arXiv:quant-ph/0209131* (2002).
  - [3] Lloyd, S., Mohseni, M. & Rebentrost, P. Quantum principal component analysis. *Nature Physics* **10**, 631–633 (2014).
  - [4] Rebentrost, P., Steffens, A., Marvian, I. & Lloyd, S. Quantum singular-value decomposition of nonsparse low-rank matrices. *Physical Review A* **97**, 6 (2018).
  - [5] Wossnig, L., Zhao, Z. K. & Prakash, A. Quantum linear system algorithm for dense matrices. *Physical Review Letters* **120**, 5 (2018).
  - [6] Farhi, E., Goldstone, J., Gutmann, S., Sipser, M., Quantum Computation by Adiabatic Evolution. *eprint arXiv:quant-ph/0001106* (2000); Farhi, E., Goldstone, J., Gutmann, S., Sipser, M., A Quantum Adiabatic Evolution Algorithm Applied to Random Instances of an NP-Complete Problem, *Science* **292**, 472-475 (2001).
  - [7] Hamma, A. & Lidar, D. A. Adiabatic preparation of topological order. *Physical Review Letters* **100**, 4 (2008).
  - [8] Mueck, L., Quantum Software, *Nature* **549**, 171 (2017); Chong, F. T., Franklin, D. &

- Martonosi, M. Programming languages and compiler design for realistic quantum hardware. *Nature* **549**, 180 (2017).
- [9] Osterloh, K., Baig, M., Santos, L., Zoller, P. & Lewenstein, M. Cold atoms in non-abelian gauge potentials: From the Hofstadter “moth” to lattice gauge theory. *Physical Review Letters* **95**, 010403 (2005); Büchler, H. P., Hermele, M., Huber, S. D. , Fisher, M. P. A. & Zoller, P., Atomic quantum simulator for lattice gauge theories and ring exchange models. *Phys. Rev. Lett.* **95**, 040402 (2005); Tagliacozzo, L., Celi, A., Orland, P., Mitchell, M. W. & Lewenstein, M. Simulation of non-abelian gauge theories with optical lattices. *Nature Communications* **4**, 8 (2013).
- [10] Byrnes, T. & Yamamoto, Y. Simulating lattice gauge theories on a quantum computer. *Physical Review A* **73**, 16 (2006).
- [11] Lamm, H., Lawrence, S., Yamauchi, Y., General Methods for Digital Quantum Simulation of Gauge Theories, *Phys. Rev. D* **100**, 034518 (2019).
- [12] Gazit, S., Assaad, F. F., Sachdev, S., Vishwanath, A. & Wang, C. Confinement transition of  $Z(2)$  gauge theories coupled to massless fermions: Emergent quantum chromodynamics and  $SO(5)$  symmetry. *Proceedings of the National Academy of Sciences of the United States of America* **115**, E6987–E6995 (2018).
- [13] Gocksch, A. Simulating lattice qcd at finite density. *Physical Review Letters* **61**, 2054–2057 (1988).
- [14] Bongiovanni, L. Numerical methods for the sign problem in lattice field theory. *eprint arXiv:1603.06458* (2016).
- [15] Gazit, S., Randeria, M. & Vishwanath, A. Emergent dirac fermions and broken symmetries in confined and deconfined phases of  $Z(2)$  gauge theories. *Nature Physics* **13**, 484–490 (2017).
- [16] Wegner, F. J. Duality in generalized ising models and phase transitions without local order parameters. *Journal of Mathematical Physics* **12**, 2259–& (1971).
- [17] Kogut, J. B. Introduction to lattice gauge-theory and spin systems. *Reviews of Modern Physics* **51**, 659–713 (1979).
- [18] Fradkin, F., Susskind, L., Order and disorder in gauge systems and magnets, *Phys. Rev. D* **17**, 2637-2658 (1978).
- [19] Sachdev, S. Topological order, emergent gauge fields, and fermi surface reconstruction. *Reports on Progress in Physics* **82** (2019).

- [20] Senthil, T. & Fisher, M. P. A. Fractionalization and confinement in the U(1) and Z(2) gauge theories of strongly correlated systems. *Journal of Physics A: Mathematical and General* **34**, L119–L125 (2001).
- [21] Kitaev, A. Y. Fault-tolerant quantum computation by anyons. *Annals of Physics* **303**, 2–30 (2003).
- [22] Kitaev, A. & Laumann, C. Topological phases and quantum computation. *eprint arXiv:0904.2771* (2009).
- [23] Fowler, A. G., Mariantoni, M., Martinis, J. M. & Cleland, A. N. Surface codes: Towards practical large-scale quantum computation. *Physical Review A* **86** (2012).
- [24] Zohar, E., Farace, A., Reznik, B. & Cirac, J. I. Digital quantum simulation of Z(2) lattice gauge theories with dynamical fermionic matter. *Physical Review Letters* **118**, 5 (2017).
- [25] Li, K. R. *et al.* Experimental identification of non-abelian topological orders on a quantum simulator. *Physical Review Letters* **118**, 5 (2017).
- [26] Luo, Z. H. *et al.* Experimentally probing topological order and its breakdown through modular matrices. *Nature Physics* **14**, 160–+ (2018).
- [27] Creutz, M., Jacobs, L. & Rebbi, C. Experiments with a gauge-invariant ising system. *Physical Review Letters* **42**, 1390–1393 (1979).
- [28] Pfeleiderer, C. Why first order quantum phase transitions are interesting. *Journal of Physics-Condensed Matter* **17**, S987–S997 (2005).
- [29] Fink, J. M., Dombi, A., Vukics, A., Wallraff, A. & Domokos, P. Observation of the photon-blockade breakdown phase transition. *Physical Review X* **7**, 9 (2017).
- [30] Juricic, V., Abergel, D. S. L. & Balatsky, A. V. First-order quantum phase transition in three-dimensional topological band insulators. *Physical Review B* **95**, 5 (2017).
- [31] Young, A. P., Knysh, S. & Smelyanskiy, V. N. First-order phase transition in the quantum adiabatic algorithm. *Physical Review Letters* **104**, 4 (2010).
- [32] Jones, T., Brown, A., Bush, I. & Benjamin, S. Quest and high performance simulation of quantum computers. *Scientific Report* **9**, 10736 (2019).
- [33] Shi, Y. & Wu, Y.-S. Perturbative formulation and nonadiabatic corrections in adiabatic quantum-computing schemes. *Physical Review A* **69**, 024301 (2004).
- [34] Fradkin, E. & Susskind, L. Order and disorder in gauge systems and magnets. *Physical Review D* **17**, 2637–2658 (1978).

- [35] Blote, H. W. J. & Deng, Y. J. Cluster Monte Carlo simulation of the transverse Ising model.  
*Physical Review E* **66**, 8 (2002).

